Upstream-Cylinder and Downstream-Cylinder Influence on the Hydrodynamics of a Four-Cylinder Group

Arun Kamath*, Mayilvahanan Alagan Chella, Hans Bihs, Øivind A. Arntsen

Department of Civil and Transport Engineering, Norwegian University of Science and Technology (NTNU), 7491 Trondheim, Norway

Journal of Waterway, Port, Coastal, and Ocean Engineering, 2016, **142** (4), pp. 04016002-1-12.
DOI: http://dx.doi.org/10.1061/(ASCE)WW.1943-5460.0000339

Abstract

The wave interaction at low Keulegan-Carpenter numbers with a group of four large cylinders arranged in the form of a square with one diagonal along the direction of wave propagation is studied with focus on the hydrodynamic effects of the most upstream and the downstream cylinders in the group. This is studied by removing them and comparing the wave forces and the free surface elevations around the three remaining cylinders with the four cylinder configuration. The theoretically predicted wave near-trapping in the case of the four cylinder group is also investigated for low and high steepness incident waves. The numerical results are compared with analytical formulae based on potential theory and differences are observed between the results for high wave steepnesses. It is observed that the downstream cylinder has a significant influence on the wave forces acting on the cylinders in the four cylinder group. It is also found that the numerical model correctly represents the wave near-trapping predicted by the analytical formula at a low incident wave steepness. For a high incident wave steepness, the diffraction regime is found to be different, with significant wave radiation from the cylinders, consequently the conditions for wave near-trapping break-down.

Keywords: cylinder groups; wave trapping; wave diffraction; REEF3D; Computational Fluid Dynamics

1 Introduction

Coastal constructions such as wave energy devices operate under low Keulegan-Carpenter numbers (KC=UT/D, where U is the magnitude of the horizontal particle velocity, T is the

*Corresponding author, arun.kamath@ntnu.no

Postprint, published in Journal of Waterway, Port, Coastal, and Ocean Engineering, doi: http://dx.doi.org/10.1061/(ASCE)WW.1943-5460.0000339

wave period and D is the diameter of the cylinder) regimes and are designed with dimensions such that their equivalent diameters D are comparable to the incident wavelength L such that $D/L > 0.2$. Under these conditions, the diffraction effects dominate the wave interaction process and significantly modify the wave field around the devices. The variation of the free surface around a group of deployed devices is an important parameter for device operation and the wave forces are important from a structural design perspective. This scenario can be studied using wave interaction with groups of large cylinders in intermediate water depths. At small distances of separation between the cylinders, each of the cylinders in the group is influenced by the wave diffraction and reflection from the neighboring cylinders. These interactions can lead to wave near-trapping. Wave near-trapping refers to the phenomenon where only a small amount of scattered wave energy in the region between closely placed cylinders is radiated outwards and a near standing wave is formed. The free surface is amplified close to the cylinders and is associated with large pressures on the cylinders, resulting in large wave forces on the cylinders. This phenomenon occurs for certain combinations of incident wavelength, cylinder array arrangement and spacing. In the case of oscillating water column wave energy devices, which operate on the principle of a water column being excited by incident waves Evans (1978), this resonant phenomenon may be used to an advantage when a deployed in a closely placed group. But, the occurrence of this phenomenon and the potential increase in the wave forces on the devices due to wave near-trapping have to be further studied.

Wave diffraction and multiple reflection amongst multiple cylinders placed in proximity has been studied using potential theory formulations by several authors such as Ohkusu (1974) Spring and Monkmeyer (1974) and Linton and Evans (1990) Walker and Taylor (2005). Malenica et al. (1999) estimated the second-order and third-order potentials to calculate higher-order forces on a cylinder array. Although these methods have provided a lot of information regarding the near-trapping phenomena at the first and the second order, the assumptions of a small incident wave amplitude, inviscid fluid and irrotational flow limit the application of these methods. Further, the interaction of high steepness waves with large cylinders can be significantly different from that with low steepness waves due to the occurrence of non-linear wave-body and wave-wave interactions. Many authors have studied the near-trapping phenomenon in the case of cylinder groups composed of four and more cylinders in a polygonal formation (Evans and Porter (1997); Walker et al. (2008)), demonstrating the importance of studying the wave diffraction effects in these cases. Huang (2004) developed a semi-analytical method to study the wave diffraction around two, three and four cylinders and computed the free surface elevations around the array and reported higher interaction in the case of a three cylinder array compared to the four cylinder array. Ohl et al. (2001) carried out experiments to study wave diffraction by an array of large cylinders and concluded that predictions from potential theory agreed well with the observations, whereas the semi-analytical theory by Malenica et al. (1999) over predicted the second-order contribution to the free surface elevations. Interaction of solitary waves with a group of four cylinders was modeled numerically by Zhao et al. (2007) using generalized Boussinesq equations. Since a solitary wave is only a crest propagating on the free surface, the interaction of periodic waves is different from the that of solitary waves and separate studies are required. Experimental investigations by Barnard et al. (1983) reported the absence of the theoretically predicted pronounced resonant response due to wave near-trapping. Duclos and Clément (2004) showed that a small amount of disorder, of the order of 0.5% of the cylinder spacing in their analysis, can substantially reduce the forces due to wave near-trapping. Thus, wave interaction

with an array of large cylinders at low KC numbers depends on many factors including the arrangement of the cylinders, the number of cylinders and the incident wave steepness. But the effect of wave steepness has not been the focus of previous studies in current literature. In this regard, further insight can be obtained by studying wave interaction with a four cylinder array with cylinders at the vertices and oriented with one diagonal arranged in the direction of wave propagation for both low and high steepness incident waves. The investigation into the variation of the free surface elevation around the four cylinder array and the wave forces on the cylinders compared to the free surface variations and wave forces in the absence of the most upstream and downstream cylinders can provide further knowledge about the changes in the wave field in the different scenarios.

In this study, the open-source Computational Fluid Dynamics (CFD) model REEF3D (Alagan Chella et al., 2015) is used to simulate the wave interaction with cylinder arrays with three and four cylinders as shown in Fig. (1). The objective of the study is to investigate the wave field around the array with four cylinders and three cylinders obtained by removing one of the cylinders from the four cylinder array, evaluate the consequences of the arrangement on the wave forces experienced by the cylinders and the difference between low and high steepness wave interaction with the cylinder arrays. The most upstream and downstream cylinders are removed from the arrangements in turns to obtain two arrangements of three cylinders to obtain insights into the influence of these cylinders on the wave forces experienced by the other cylinders in the array. The free surface in the vicinity of the cylinders and the wave forces on the cylinders are computed for incident waves for two different incident wavelengths at both low and high wave steepnesses are studied. The formula by Linton and McIver (2001) is used for the validation of the numerical results for the four cylinder array at a low incident wave steepness.

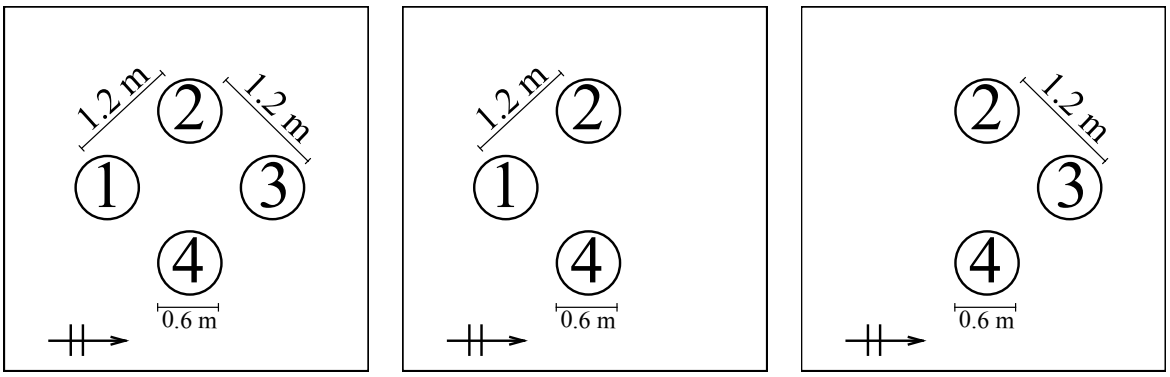

(a) setup 1 (b) setup 2 (c) setup 3

Figure 1: Different arrangements used in the study

2 Numerical Model

2.1 Governing equations

The incompressible Reynolds-averaged Navier-Stokes (RANS) equations together with the continuity equation are used in the numerical wave tank in REEF3D:

$$\frac{\partial u_i}{\partial x_i} = 0 \tag{1}$$

$$\frac{\partial u_i}{\partial t} + u_j \frac{\partial u_i}{\partial x_j} = -\frac{1}{\rho}\frac{\partial p}{\partial x_i} + \frac{\partial}{\partial x_j}\left[(\nu + \nu_t)\left(\frac{\partial u_i}{\partial x_j} + \frac{\partial u_j}{\partial x_i}\right)\right] + g_i \tag{2}$$

where u is the velocity, ρ is the density of the fluid, p is the pressure, ν is the kinematic viscosity, ν_t is the eddy viscosity and g the acceleration due to gravity.
The projection method (Chorin, 1968) is used for pressure treatment and a preconditioned BiCGStab solver (van der Vorst, 1992) is used to solve the resulting Poisson pressure equation. Turbulence modeling is carried out using the two equation k-ω model proposed by Wilcox (1994) with transport equations for turbulent kinetic energy k and specific turbulence dissipation rate ω given by:

$$\frac{\partial k}{\partial t} + u_j \frac{\partial k}{\partial x_j} = \frac{\partial}{\partial x_j}\left[\left(\nu + \frac{\nu_t}{\sigma_k}\right)\frac{\partial k}{\partial x_j}\right] + P_k - \beta_k k\omega \tag{3}$$

$$\frac{\partial \omega}{\partial t} + u_j \frac{\partial \omega}{\partial x_j} = \frac{\partial}{\partial x_j}\left[\left(\nu + \frac{\nu_t}{\sigma_\omega}\right)\frac{\partial \omega}{\partial x_j}\right] + \frac{\omega}{k}\alpha P_k - \beta\omega^2 \tag{4}$$

where, P_k is the production rate and closure coefficients $\sigma_k = 2$, $\sigma_\omega = 2$, $\alpha = 5/9$, $\beta_k = 9/100$, $\beta = 3/40$. Wall functions for k and ω are defined as follows:

$$k = \frac{u_T}{\sqrt{\beta_k}}, \qquad w = \frac{k^{1/2}}{(\beta_k)^{1/4}\kappa y} \tag{5}$$

where κ is the Karman constant, u_T is the friction velocity (Wilcox, 1994). The turbulence production based on the strain rate in the numerical wave tank results in overproduction of turbulence because of the large strain in the flow due to wave propagation. Eddy viscosity is bounded as shown by Durbin (2009) are used to avoid this as shown below:

$$\nu_t = min\left(\frac{k}{\omega}, \sqrt{\frac{2}{3}}\frac{k}{|\mathbf{S}|}\right) \tag{6}$$

where $\mathbf{S}$ stands for strain from the source terms in the transport equations. The strain tensor is defined as:

$$S_{ij} = \frac{1}{2}\left(\frac{\partial u_j}{\partial x_i} + \frac{\partial u_i}{\partial x_j}\right) \tag{7}$$

In a two-phase CFD model, the large difference in density at the interface between air and water causes an overproduction of turbulence at the interface because the standard k-ω model does not account for the free surface where the turbulent eddies from the water are

dissipated. This effect accounted for by defining the specific turbulent dissipation term around the interface ω_s as shown by Naot and Rodi (1982):

$$\omega_s = \frac{c_\mu^{-\frac{1}{4}}}{\kappa} k^{\frac{1}{2}} \cdot \left(\frac{1}{y'} + \frac{1}{y^*} \right) \tag{8}$$

where $c_\mu = 0.07$ and $\kappa = 0.4$. The variable y' is the virtual origin of the turbulent length scale, and was empirically found to be 0.07 times the mean water depth Hossain and Rodi (1980). Including the distance y^* from the nearest wall gives a smooth transition from the free surface value to the wall boundary value of ω.

2.2 Free Surface

The free surface is determined with the level set method, where the zero level set of the signed distance function $\phi(\vec{x}, t)$ is used to represent the interface between air and water (Osher and Sethian, 1988). The level set function gives the shortest distance from the interface for all the points in the flow domain. The sign of the function distinguishes between the two fluids across the interface as shown in Eq. (9):

$$\phi(\vec{x}, t) \begin{cases} > 0 & if\ \vec{x}\ is\ in\ phase\ 1 \\ = 0 & if\ \vec{x}\ is\ at\ the\ interface \\ < 0 & if\ \vec{x}\ is\ in\ phase\ 2 \end{cases} \tag{9}$$

The level set function is moved under the influence of an external velocity field u_j with the convection equation in Eq. (10):

$$\frac{\partial \phi}{\partial t} + u_j \frac{\partial \phi}{\partial x_j} = 0 \tag{10}$$

The level set function loses its signed distance property on convection and is reinitialized after every iteration using a partial differential equation based reinitialisation procedure by Peng et al. (1999) to regain its signed distance property.

2.3 Discretization schemes

The fifth-order conservative finite difference Weighted Essentially Non-Oscillatory (WENO) scheme proposed by Jiang and Shu (1996) is applied for the discretization of the convective terms of the RANS equation. The level set function, turbulent kinetic energy and the specific turbulent dissipation rate are discretized using the Hamilton-Jacobi formulation of the WENO scheme by Jiang and Peng (2000). The WENO scheme is a minimum third-order accurate and numerically stable even in the presence of large gradients. Time advancement for the momentum and level set equations is carried out using a Total Variation Diminishing (TVD) third-order Runge-Kutta explicit time scheme proposed by Shu and Osher (1988). Adaptive time stepping is employed to satisfy the CFL (Courant-Friederichs-Lewy) criterion based on the maximum velocities in the domain and the source term contributions to the Navier-Stokes equations. This ensures numerical stability and accuracy throughout the simulation with an optimal value of time step size. A first-order implicit Euler scheme is used for the time advancement of the turbulent kinetic energy and the specific turbulent dissipation, as these

variables are mostly source term driven with a low influence of the convective terms. Diffusion terms of the velocities are also subjected to implicit treatment in order to remove the diffusion terms from the CFL criterion.

The numerical model uses a uniform Cartesian grid for the spatial discretization together with the Immersed Boundary Method (IBM) to represent the irregular boundaries in the domain. Berthelsen and Faltinsen (2008) developed the local directional ghost cell IBM to extend the solution smoothly in the same direction as the discretization, which is adapted to three dimensions in the current model. REEF3D is fully parallelized using the domain decomposition strategy and MPI (Message Passing Interface).

2.4 Wave generation and absorption

The numerical wave tank uses the relaxation method (Larsen and Dancy, 1983) for wave generation and absorption. This method requires a certain length of the wave tank to be reserved as wave generation and absorption zones. Relaxation functions are used to moderate the velocity and the free surface using a wave theory in the relaxation zones with Eq. (11):

$$\begin{aligned} u_{relaxed} &= \Gamma(x) u_{analytical} + (1 - \Gamma(x)) u_{computational} \\ \phi_{relaxed} &= \Gamma(x) \phi_{analytical} + (1 - \Gamma(x)) \phi_{computational} \end{aligned} \tag{11}$$

where $\Gamma(x)$ is the relaxation function and $x \in [0, 1]$ is the x-coordinate scaled to the length of the relaxation zone. The relaxation function proposed by Jacobsen et al. (2012), shown in Eq. (12) is used in the numerical model.

$$\Gamma(x) = 1 - \frac{e^{(1-x)^{3.5}} - 1}{e - 1} \tag{12}$$

The numerical model can simulate waves defined by several wave theories such as linear, $2nd$-order Stokes, $5th$-order Stokes, Cnoidal and solitary wave theory depending on the case being studied. The wave theory used for wave generation by the relaxation method is chosen according to the wave steepness and the water depth in the simulation. In the current study, waves with steepness $H/L = 0.003$ are generated using the linear theory and with steepness $H/L = 0.06$ and 0.10 are generated using the $5th$-order Stokes wave theory. Typically, the wave generation zone is one wavelength long and the absorption zone is two wavelengths long. In the wave generation zone, the computational values of velocity and free surface are raised to the analytical values prescribed by wave theory. The generation zone releases waves into the working zone of the tank, where the objects to be studied are placed. The relaxation function in the generation zone also absorbs reflections from structures in the wave tank and prevents them from affecting the generated waves. At the end of the tank, the wave enters the numerical beach. Here, the computational values of velocity and free surface are reduced to zero in a smooth manner. This simulates the effect of a beach, where the wave energy is removed from the wave tank and avoids reflections. In a three-dimensional numerical wave tank, the relaxation functions for wave generation and absorption form the boundary conditions at the two ends of the tank. No-slip wall boundary conditions are enforced on the side walls and the bottom of the wave tank. The top of the wave tank is open to the atmosphere and symmetry boundary condition is applied.

3 Calculation of Wave Forces

3.1 Numerical evaluation of wave forces

The numerical model evaluates the wave force F on an object as the integral of the pressure p and the surface normal component of the viscous shear stress tensor τ on the object according to Eq. (13):

$$F = \int_{\Omega} (-\mathbf{n}p + \mathbf{n} \cdot \tau) d\Omega \tag{13}$$

where $\mathbf{n}$ is the unit normal vector pointing into the fluid and Ω is the surface of the object. This is readily accomplished by the numerical model as the values for the pressure and shear stress are available at every point in the domain at any given time of the simulation. The no-slip wall boundary condition is applied on the surface of the object and the effect of the boundary layer is modeled through the wall laws in the turbulence model.

3.2 Analytical formula for wave forces

Potential theory is used to obtain the wave diffraction potential and calculate the force on a single cylinder using the equation presented by MacCamy and Fuchs (1954), shown in Eq. (14):

$$|F| = \left| \frac{4\rho g i a \ tanh(kd)}{k^2 H_1'(kr)} \right| \tag{14}$$

where $i = \sqrt{-1}$, a is the incident wave amplitude, $k = 2\pi/L$ the wave number, d the water depth and H_1' the first derivative of the Hankel function of the first kind and r the radius of the cylinder. The parameter kr represents the ratio of the diameter of the cylinder to the incident wavelength and thus a measure of the diffraction, with higher values of kr signifying a stronger diffraction regime.
An extension of the diffraction theory proposed by Linton and McIver (2001) to calculate wave forces on multiple cylinders placed in proximity is presented in Eq. (15):

$$A_m^l + \sum_{\substack{j=1 \\ \neq l}}^{N} \sum_{n=-M}^{M} A_j^n Z_n^j e^{i(n-m)\alpha_{jl}} H_{n-m}(kR_{jl}) = -I_l e^{im(\frac{\pi}{2}-\beta)}$$

$$l = 1, \ldots, N, \ m = -M, \ldots, M. \tag{15}$$

where, M is the order of the solution, N is the number of cylinders, I is the incident wave potential, β is the angle of wave propagation with respect to the x-axis, H is the Hankel function of the first kind, R_{jl} is the length of the line joining the centers of the jth and the lth cylinder, α_{jk} is the angle between the x-axis and the line joining the centers of the cylinders and $Z = J'(kr_j)/H'(kr_j)$, where J is the Bessel function of the first kind. The unknown coefficients A are to be evaluated. This results in a set of $N(2M+1)$ equations. Linton and McIver (2001) suggest that a value of $M = 6$ provides sufficiently accurate solutions and is used in the equations to obtain the analytical prediction of wave forces for low steepness incident waves. The unknown coefficients A are evaluated by solving Eq. (15) and the first-order wave force magnitudes $|F^j|$ on the jth cylinder are obtained using Eq. (16):

$$\left| \frac{F^j}{F} \right| = \frac{1}{2} \left| A_{-1}^j \pm A_1^j \right| \tag{16}$$

The subtraction of the coefficients on the right hand side gives the wave force along the x-axis and the addition of the terms gives the wave force along the y-axis. In the current study, the angle of incidence $\beta = 0$ and the waves propagate along the x-axis.

4 Results and Discussion

Wave interaction with three arrangements of the cylinder array as shown in Fig. (1) with two different incident wavelengths at small and large wave steepness are considered. The first arrangement consists of four cylinders placed with a diagonal along the direction of wave propagation (Fig. 1a). In the second arrangement, the downstream cylinder on the inline diagonal is removed, resulting in a triangular arrangement of three cylinders (Fig. 1b) and in the third setup, a triangular arrangement is obtained by removing the upstream cylinder on the inline diagonal (Fig. 1c). Cylinders of diameter $D = 0.60$ m are arranged at the vertices of a square of side $2D$=1.20 m in a water depth of $d = 0.60$ m. The center-to-center distance is taken to be $2D$ to maintain the same distance used in the results presented by Linton and Evans (1990). Also, in the case of wave energy device arrays, this is a suitable of separation between devices in a group. The numerical wave tank used for the simulations is 16 m long, 8 m wide and 1.20 m high with a grid size of $dx = 0.025$ m resulting in 9.83 million cells. The computational grid around a cylinder in the wave tank is shown in Fig. (2). The width of the wave tank is chosen such that the reflections from the side walls of the tank do not significantly influence the results in the wave tank. The outer surface of the cylinders closest to the wall (2 and 4) are 2.55D from the wall and the surface of the cylinders in the center (1 and 4) are 6.16D from the side wall. An overview of the simulations carried out is listed in Table 1. According to the equations by Linton and Evans (1990), wave interaction with the arrangement of four cylinders in Fig. (1a) results in wave near-trapping for a diffraction parameter $kr = 1.70$. Thus, simulations are carried out for $kr = 0.94$ to simulate the wave interaction away from wave near-trapping (setup A1) and for $kr = 1.70$ (setup B1) to simulate wave near-trapping at a low incident wave steepness of $H/L = 0.004$. Further, the wave interaction for the same values of the diffraction parameter kr is simulated at a higher wave steepness of $H/L = 0.060$ to investigate the differences in the diffraction regime and wave forces from that seen for the low incident wave steepness.

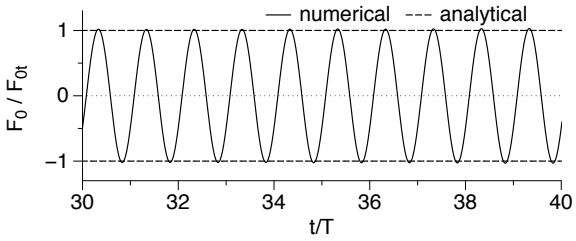

Figure 2: Computational mesh around a cylinder in the numerical wave tank

At first, the numerical computation of the wave forces on cylinders is validated by simulating wave interaction with a single cylinder and a group of four cylinders (setup A1) with low steepness incident waves ($H/L = 0.004$) of wavelength $L = 2.00$ m and height $H = 0.008$ m. The numerical results for the single cylinder $F_0 = 16.20$ N are compared with the analytically

Table 1: Details of the setups used in the different simulations

No.	H (m)	L (m)	KC	H/L	kr	$F_0(N)$	Arrangement
A1							Setup 1
A2	0.008	2.00	0.04	0.004	0.94	16.20	Setup 2
A3							Setup 3
B1							Setup 1
B2	0.004	1.11	0.02	0.004	1.70	3.90	Setup 2
B3							Setup 3
C1							Setup 1
C2	0.120	2.00	0.66	0.06	0.94	178.20	Setup 2
C3							Setup 3
D1							Setup 1
D2	0.066	1.11	0.35	0.06	1.70	50.50	Setup 2
D3							Setup 3
E1							Setup 1
E2	0.20	2.00	1.10	0.10	0.94	310.60	Setup 2
E3							Setup 3
F1							Setup 1
F2	0.11	1.11	0.57	0.10	1.70	45.40	Setup 2
F3							Setup 3

expected values using the MacCamy-Fuchs theory $F_{0t} = 15.90$ N in Eq. (14) in Fig. (3) with only a difference of 1.8%. In the case of the four cylinders, the computed forces on each of the cylinders is compared with the analytical prediction using Eq. (16) in Fig. (4) and a good agreement is seen for all the four cylinders, with differences less than 2.0%.

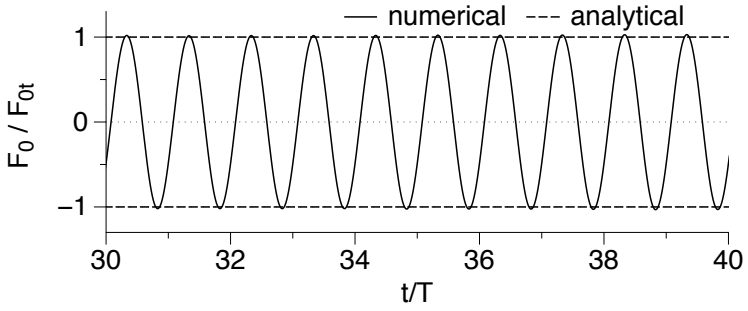

Figure 3: Comparison of numerical and analytical wave forces on a single cylinder for $H =$ 0.008 m and $L = 2.00$ m

In the following sections, the wave interaction with the three setups illustrated in Fig. (1) is investigated with low and high steepness waves for two different wavelengths.

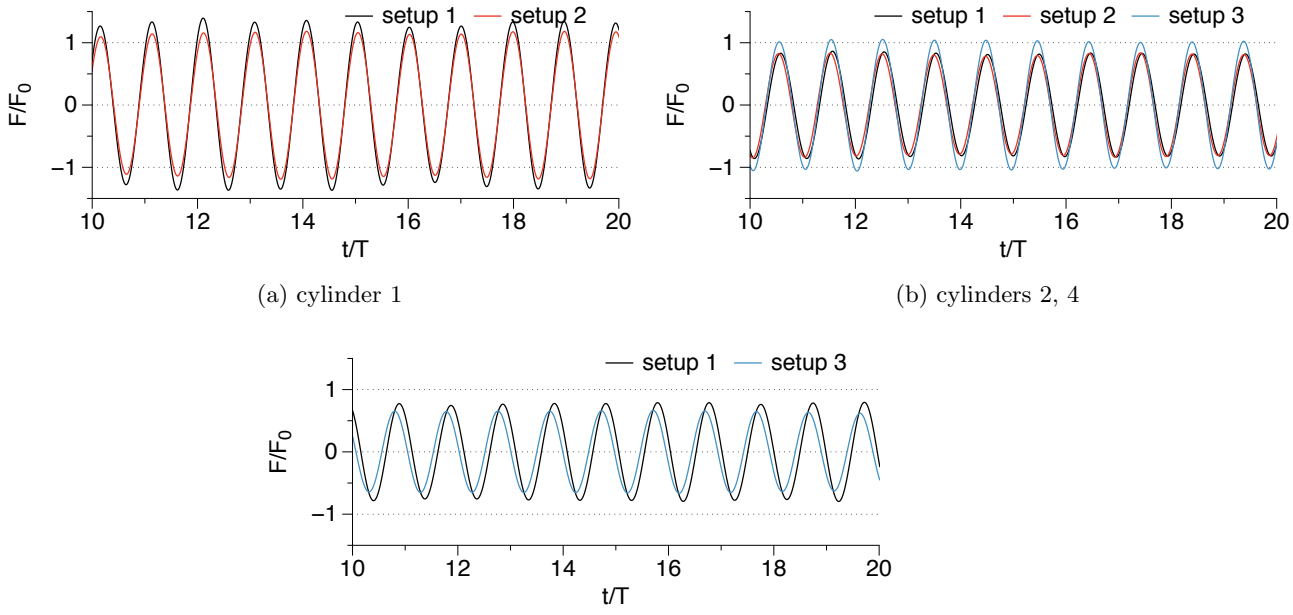

(a) cylinder 1

(b) cylinders 2, 4

(c) cylinder 3

Figure 4: Comparison of the numerical and analytical wave forces on the four cylinders in setup A1 with $H = 0.008$ m and $L = 2.00$ m for $kr = 0.94$

4.1 Wave interaction with incident waves of low steepness, $H/L = 0.004$

The wave forces on cylinders for the setups A1, A2 and A3 with incident wavelength $L = 2.00$ m and height $H = 0.008$ m resulting in a low wave steepness of $H/L = 0.004$ and diffraction parameter $kr = 0.94$ are computed as listed in Table (1). The computed wave forces on each cylinder are scaled to the numerically determined force on a single cylinder, $F_0 = 16.20$ N and presented in Fig. (5). It is seen from Fig. (5a) that cylinder 1 experiences the highest wave forces in both setups 1 and 2. It is also observed that in the presence of the downstream cylinder 3, in setup 1, the wave force on the upstream cylinder 1 is higher with $1.30F_0$ compared to $1.15F_0$ in the absence of the downstream cylinder 3 in setup 2. In the case of cylinders 2 and 4, the highest wave forces are experienced in setup 3, when the upstream cylinder 1 is removed from the arrangement as seen in Fig. (5b). In the presence of the upstream cylinder 1, cylinders 2 and 4 experience similar wave forces for both setups 1 and 2. From Fig. (5c), the downstream cylinder 3 experiences the highest wave forces in the presence of the upstream cylinder 1 and lower forces in the absence of the upstream cylinder. Thus, in the four cylinder arrangement shown in Fig. (1a), the presence of the upstream cylinder reduces the wave forces on cylinders 2 and 4 behind it, but leads to a higher wave force on the downstream cylinder 3. From the results presented above, this can be attributed to the increased total pressure acting on the downstream cylinder 3 due to the inline presence of the upstream cylinder 1.

Further, the diffraction parameter is changed to $kr = 1.70$ and the wave forces on the cylinders for the setups B1, B2 and B3 with incident wavelength $L = 1.11$ m and height $H = 0.004$ m (H/L=0.0036) are computed. In this arrangement, the equations by Linton and

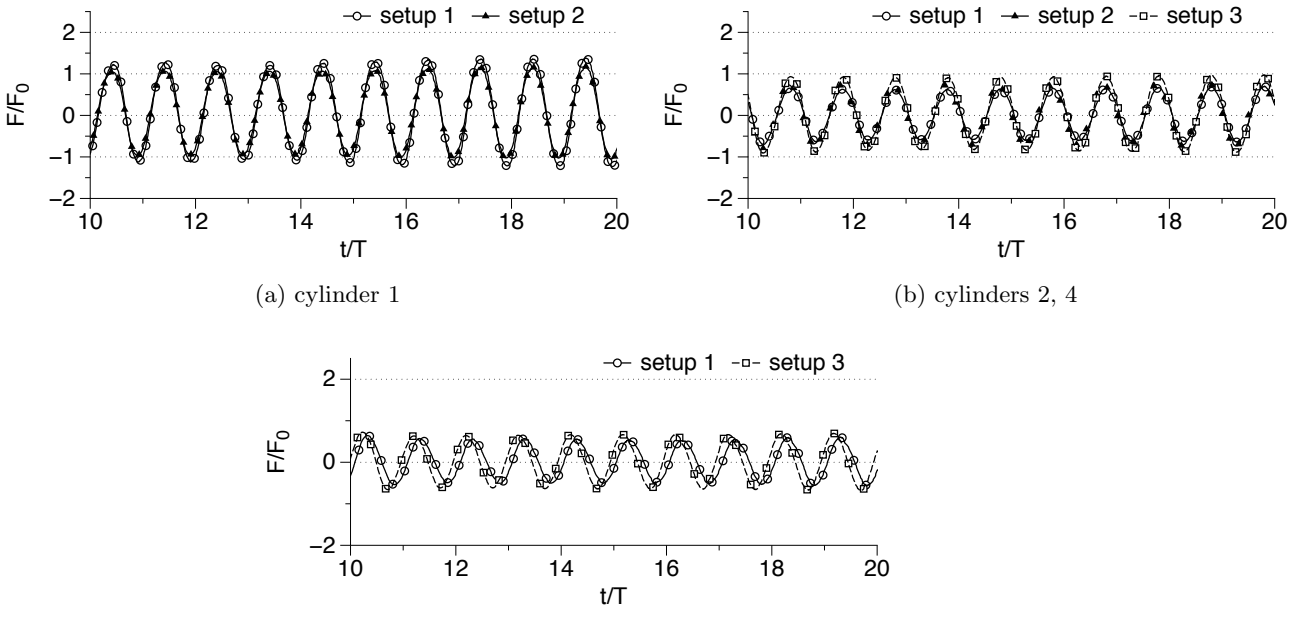

(a) cylinder 1

(b) cylinders 2, 4

(c) cylinder 3

Figure 5: Comparison of wave forces on each of the cylinders in setups A1, A2 and A3 for steepness $H/L = 0.004$ with $H = 0.008$ m and $L = 2.00$ m for $kr = 0.94$

McIver (2001) predict large wave forces on the cylinders in setup 1, due to near-wave trapping. The numerical results follow with this prediction and the wave forces on all four cylinders in setup 1 experiences larger forces than the wave force computed for a single cylinder, $F_0 = 3.90$ N. In the case of cylinder 1, the wave force is $2.00F_0$ in setup 1, whereas it is lowered to $1.30F_0$ when the downstream cylinder is removed in setup 2 as seen in Fig. (6a). For cylinders 2 and 4, the wave forces are similar ($1.10F_0$) in all the three setups from Fig. (6b). The downstream cylinder 3 also experiences similar forces of $1.60F_0$ both in the presence and absence of the upstream cylinder in Fig. (6c). So, under conditions resulting in near wave trapping for the four cylinder arrangement, the wave forces on the upstream cylinder is highly influenced by the presence of the downstream cylinder but the effect of the upstream cylinder on the other cylinders in the arrangement is negligible.

From the simulations presented above, it is observed that the wave forces on cylinders in different arrangements is influenced both by the neighboring cylinders and the incident wavelength. The effect of wave near-trapping for setup 1 for diffraction parameter $kr = 1.70$ predicted by the analytical formula (Eq. 16) is replicated in the simulation for setup B1. Under conditions resulting in near-trapping of incident waves for the four cylinder arrangement, the wave force on the upstream cylinder is two times the force on a single cylinder. On the hand, the force on cylinder 1 is reduced in the absence of the downstream cylinder 3 in setup B2. The wave forces on the other cylinders are slightly influenced by the presence of the upstream cylinder and experience forces higher than the force on a single cylinder in all the arrangements. With diffraction parameter $kr = 0.94$, there is no near-trapping of waves in setup A1 and the presence of the upstream cylinder influences all the other cylinders

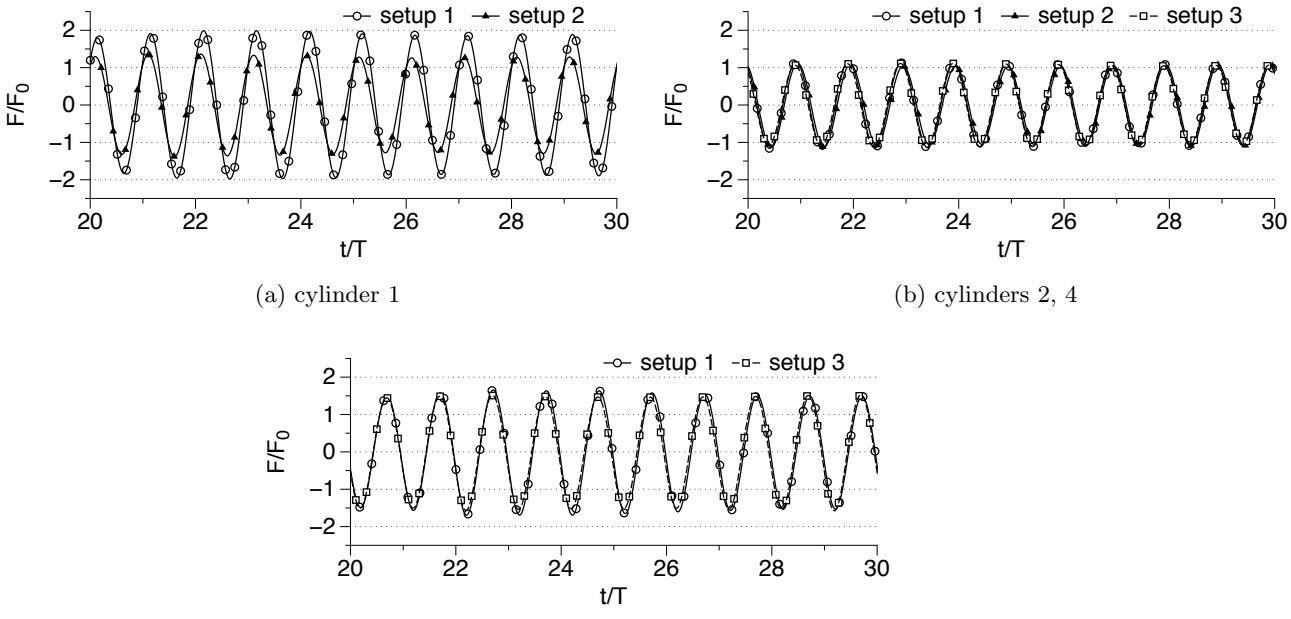

(a) cylinder 1

(b) cylinders 2, 4

(c) cylinder 3

Figure 6: Comparison of wave forces on each of the cylinders in setups B1, B2 and B3 for steepness $H/L = 0.004$ with $H = 0.004$ m and $L = 1.11$ m for $kr = 1.70$

in the arrangement as seen from the results for setups A2 and A3. The upstream cylinder itself experiences higher wave forces in the presence of the downstream cylinder. In addition, the downstream cylinder experiences higher forces in the presence of the upstream cylinder. So, away from conditions leading to wave near-trapping, the neighboring cylinders have a significant influence on the wave forces experienced by a cylinder in the group.

To obtain a better understanding of the wave regime around the cylinders, the free surface elevation around the cylinder arrays is studied when the incident wave crest is in the region enclosed by the cylinders. The diffracted waves in the region between the cylinders in setups B1-B3 is presented in Fig. (7). In setup B1 with four cylinders (Fig. 7a and 7b), a higher free surface elevation in the region in between the cylinders is seen along with a deep trough in front of cylinder 3. The wave near-trapping in this case results in large variations in the free surface in the region in between the region. The large difference in the free surface elevations correspond to large differences in the pressure around cylinders 1 and 3, resulting in large forces on the cylinders. On removing the downstream cylinder 3 from the arrangement in setup B2 (Fig. 7c and 7d), the region in between the cylinders has lower free surface elevations than in setups B1 and B2. In the absence of the downstream cylinder 3, wave trapping in the region between the cylinders does not occur and cylinder 1 experiences lower forces. The free surface elevation in the immediate vicinity of cylinders 2 and 4 is largely unaltered from the pattern seen for setup B1. In Fig. (7e and 7f), when cylinder 1 is removed, the high free surface elevation is around cylinders 2 and 4 is similar to setup B1 except for the lower free surface elevation in the region in the center. This shows that the pressure difference around cylinders 2 and 4 is similar in all the three arrangements and justifies the similar wave

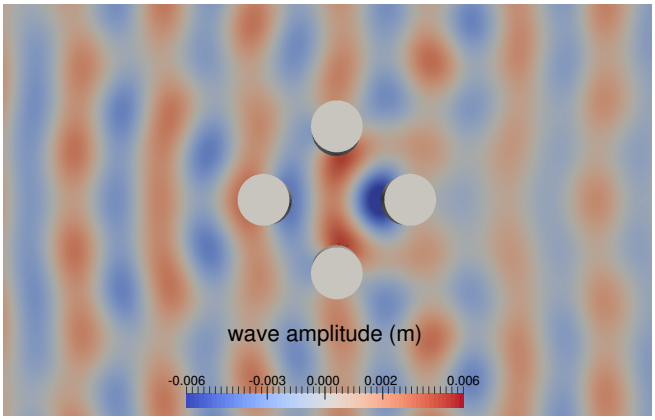

(a) t/T=34.5 for setup B1

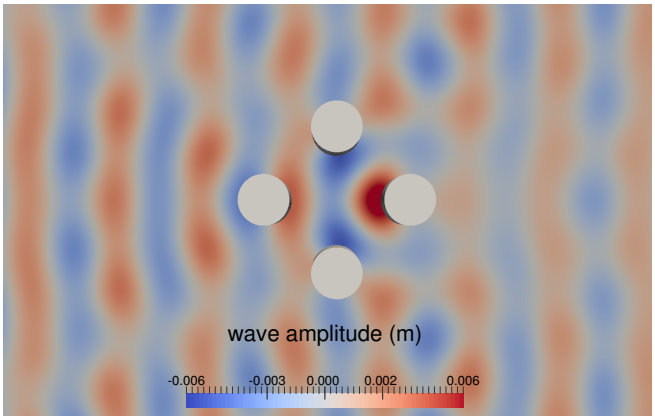

(b) t/T=35.0 for setup B1

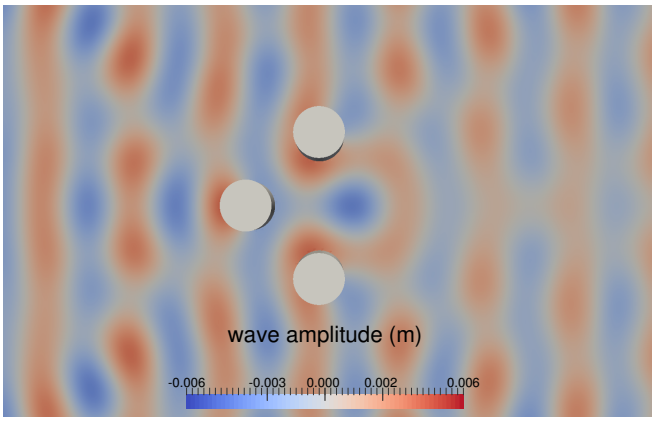

(c) t/T=34.5 for setup B2

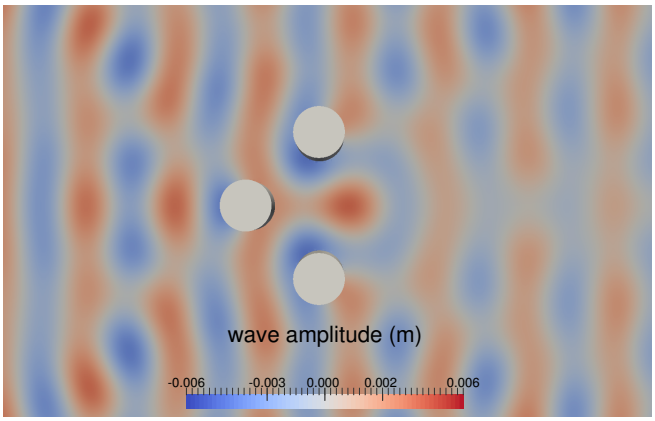

(d) t/T=35.0 for setup B2

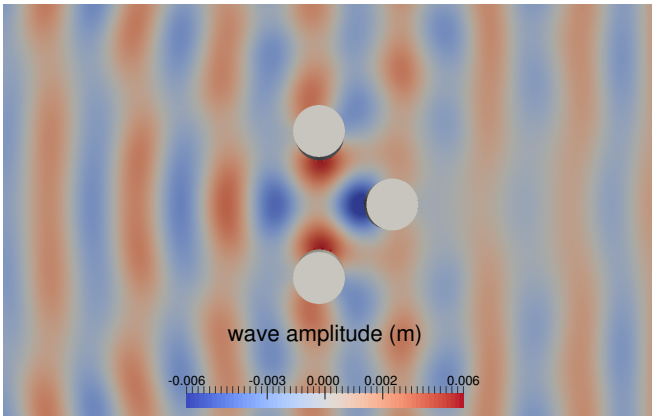

(e) t/T=34.5 for setup B3

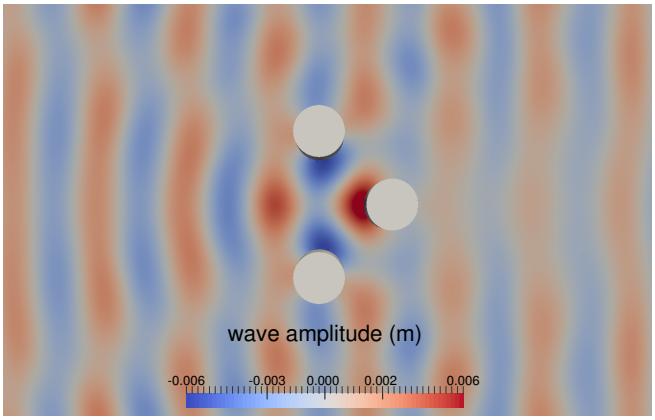

(f) t/T=35.0 for setup B3

Figure 7: Free surface elevations in the part of the domain around the cylinders for low steepness $H/L = 0.004$ in setups B1, B2 and B3 with $H = 0.004$ m, $L = 1.11$ m, for $kr = 1.70$

forces computed using Eq. (13) for cylinders 2 and 4 for all the arrangements. The free surface

elevation around the downstream cylinder is also similar to to that in setup B1, corresponding to similar pressure differences and resulting in similar forces on the downstream cylinder 3 in both setups B1 and B3.

4.2 Wave interaction with incident waves of high steepness, $H/L = 0.06$

In order to investigate the difference in the wave interaction with the cylinder groups under the the influence of high steepness incident waves, simulations are carried out with the same wavelengths as in the previous section but with a higher incident wave steepness of $H/L = 0.06$.

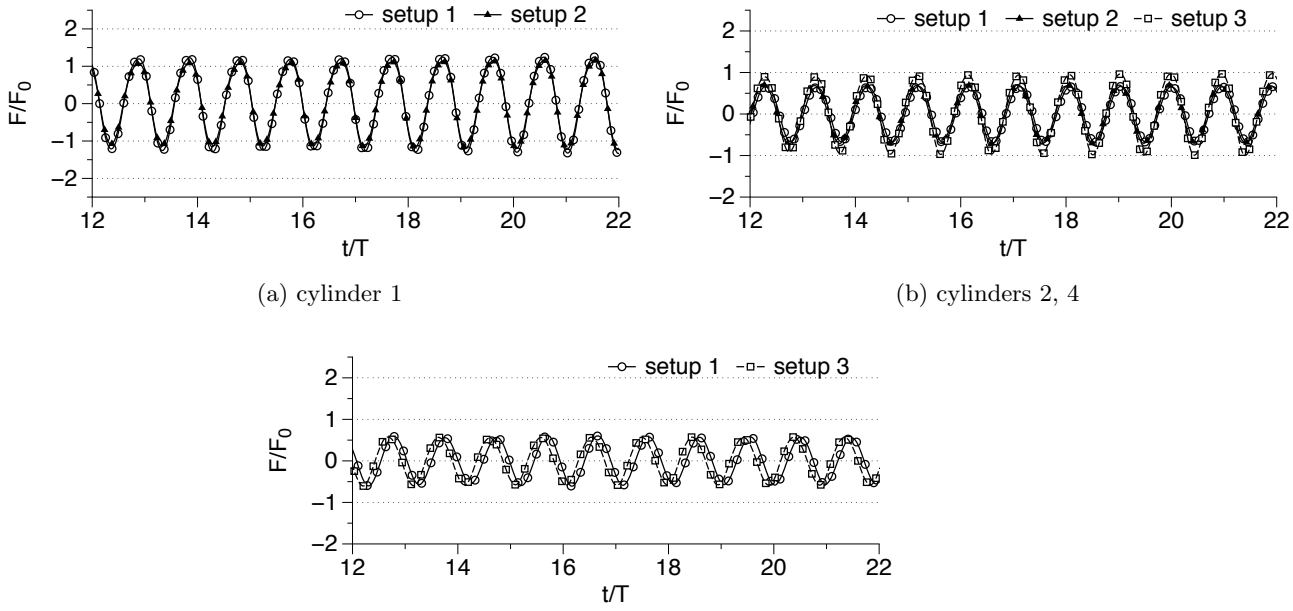

(a) cylinder 1

(b) cylinders 2, 4

(c) cylinder 3

Figure 8: Comparison of wave forces on each of the cylinders in setups C1, C2 and C3 for steepness $H/L = 0.06$ with $H = 0.12$ m and $L = 2.00$ m for $kr = 0.94$

The wave forces on all the cylinders in setups C1, C2 and C3 ($kr = 0.94$) with incident wavelength $L = 2.00$ m, height $H = 0.12$ m are presented in Fig. (8). From Fig. (8a), the wave forces on the upstream cylinder 1 are higher ($1.60F_0$) in the presence of the downstream cylinder 3 in setup 1, than in the absence of the downstream cylinder 3 in setup 2 ($1.40F_0$). Cylinders 2 and 4 experience similar forces in all the three setups, almost the same force as that on a single cylinder, $F_0 = 178.20$ N, but with slightly higher forces on cylinders 2 and 4 in the absence of the upstream cylinder as seen in Fig. (8b). The downstream cylinder 3 experiences a wave force of $0.75F_0$ in the presence of the upstream cylinder 1 and a lower force of $0.55F_0$ in the absence of the upstream cylinder in Fig. (8c). It is also observed that the wave forces on the downstream cylinder are the lowest in the group and lesser than the force on a single cylinder.

Further, the wave forces computed on all the cylinders in setups D1, D2 and D3 ($kr = 1.70$) with incident wavelength $L = 1.11$ m and height $H = 0.066$ m (H/L=0.06) are presented in

Fig. (9) scaled to $F_0 = 50.50$ N. The upstream cylinder 1 experiences wave forces of about $1.20F_0$ both in the presence and absence of the downstream cylinder 3. Cylinders 2 and 4 experience similar forces of about $0.90F_0$ in all the arrangements. The downstream cylinder 3 experiences wave forces of about $0.85F_0$. Thus, also in this case, the upstream cylinder experiences the highest forces in all the arrangements and all the other cylinders experience forces lower than F_0 for all arrangements.

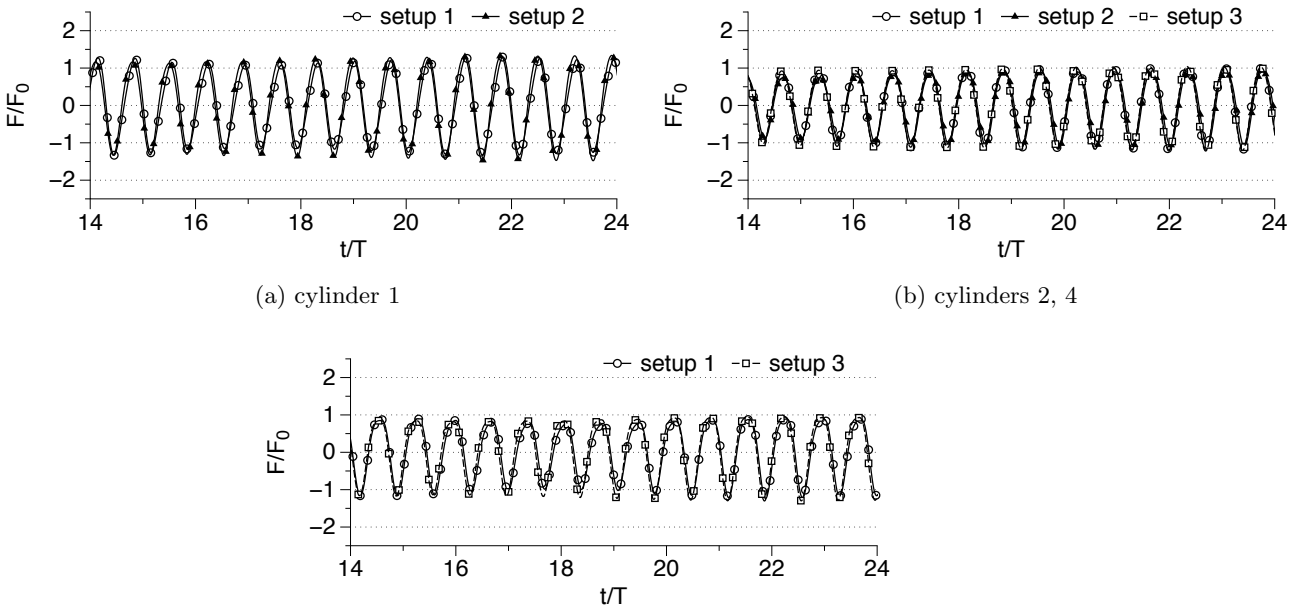

(a) cylinder 1

(b) cylinders 2, 4

(c) cylinder 3

Figure 9: Comparison of wave forces on each of the cylinders in setups D1, D2 and D3 for steepness $H/L = 0.06$ with $H = 0.066$ m and $L = 1.11$ m for $kr = 1.70$

From the simulations for high steepness incident waves, the upstream cylinder experiences the highest forces and all the other cylinders in the arrangement experience lower forces. The large wave forces on the cylinders seen in setup B1 with low incident wave steepness, due to wave near-trapping is not seen for the high steepness waves in setup D1 for the same diffraction parameter $kr = 1.70$. This points towards the break-down of the wave near-trapping condition at higher wave steepnesses.

Further insight is obtained regarding the wave diffraction effects for higher steepness incident waves by studying the free surface elevations in the region around the cylinder arrays for setups D1-D3, with incident wavelength $L = 1.11$ m and wave steepness $H/L = 0.06$ in Fig. (10). The formation of multiple semi-circular diffracted waves around the cylinders in all three setups is seen. For setup D1 (Fig. 10a), the region in between the cylinders does not show large free surface elevations and it can be concluded that the near-trapping phenomenon does not occur in this case. As a result, the cylinders do not experience extremely high wave forces in comparison to the wave force on a single cylinder. When the downstream cylinder 3 is removed from the cylinder array in setup D2 (Fig. 10c), the wave diffraction patterns around the cylinder is similar to that in setup D1 and the cylinders experience similar forces

in both arrangements. In Fig. (10e), on removing cylinder 1, high free surface are seen but restricted to small regions around cylinder 2 and 4. The free surface elevations in front of cylinder 3 is similar to that seen in setup D1 with four cylinders and thus, it experiences similar forces in both arrangements.

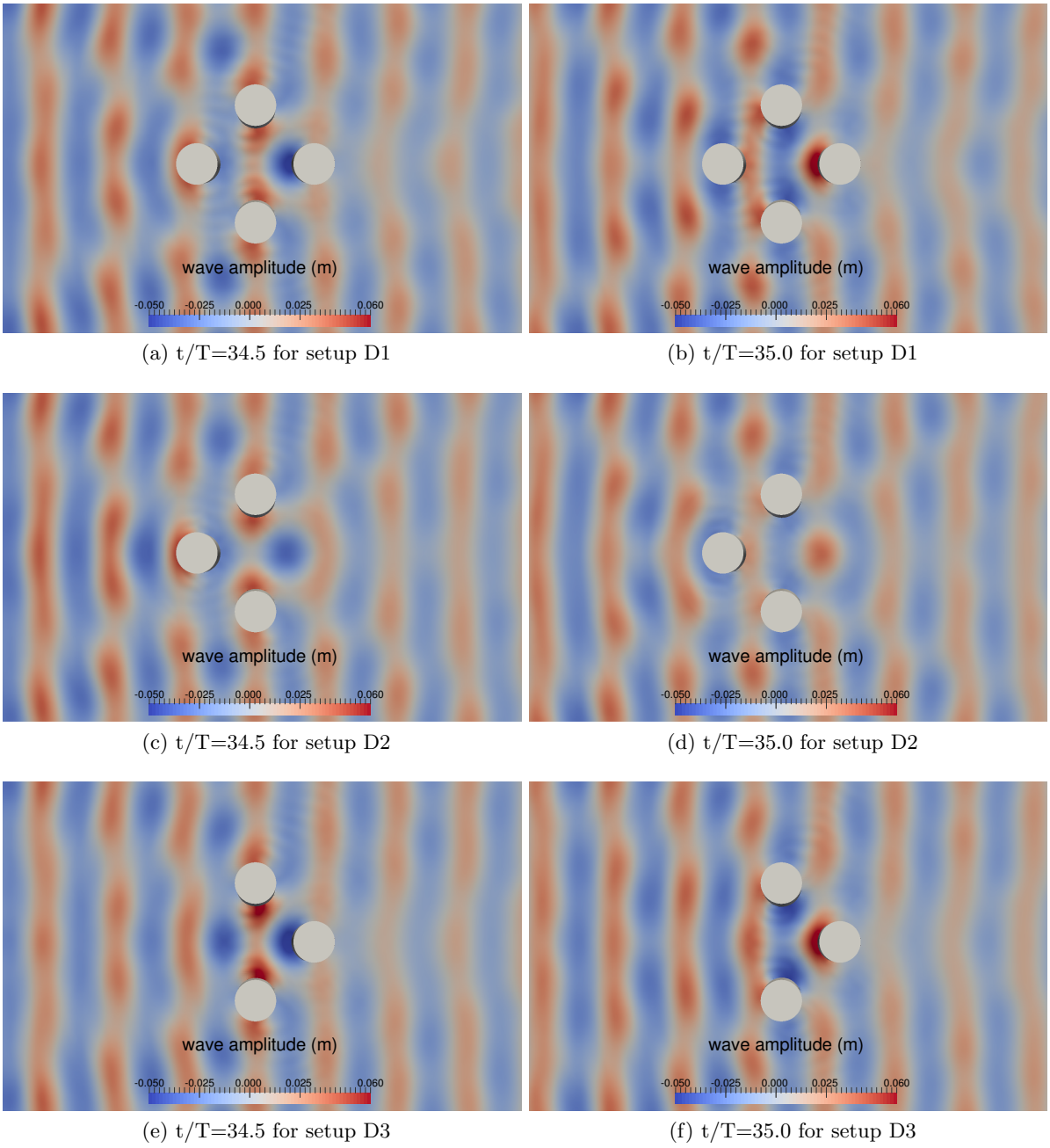

(a) t/T=34.5 for setup D1

(b) t/T=35.0 for setup D1

(c) t/T=34.5 for setup D2

(d) t/T=35.0 for setup D2

(e) t/T=34.5 for setup D3

(f) t/T=35.0 for setup D3

Figure 10: Free surface elevation in the part of the domain around the cylinders for steepness $H/L = 0.06$ in setups D1, D2 and D3 with $H = 0.066$ m, $L = 1.11$ m for $kr = 1.70$

4.3 Wave interaction with incident waves of very high steepness, $H/L = 0.10$

The deviation of the numerical results for wave forces from the prediction using the analytical formula is already seen at a higher wave steepness of $H/L = 0.06$ compared to $H/L = 0.004$. To further explore the effect of high steepness waves, simulations are carried out with an even higher steepness of $H/L = 0.10$ for both the incident wavelengths $L = 2.00$ m (cases E1-E3) and $L = 1.11$ m (cases F1-F3) for all the three different configurations of the cylinders considered in the study.

The computed wave force on each cylinder in the three setups for an incident wave height $H = 0.20$ m and wavelength $L = 2.00$ m is presented in Fig. (11) and scaled to the wave force on a single cylinder $F_0 = 310.6$ N. It is seen from Fig. (11a) that the wave force on the upstream cylinder 1 in the presence of the downstream cylinder 3 in setup 1 is slightly higher ($1.25F_0$) than in the absence the downstream cylinder in setup 2 ($1.07F_0$). This is similar to the observation made in cases C1-C3 for a wave steepness of $H/L = 0.06$. In the case of cylinders 2 and 4, the similar wave forces are computed for setups 1 and 2 in the presence and absence of the downstream cylinder. But slightly higher forces are experienced in the absence of the upstream cylinder 1 from Fig. (11b). At this incident wave steepness, the absence of the upstream cylinder slightly increases the total pressure on cylinders 2 and 4 resulting in higher wave forces. This is also similar to the trend seen in the case of incident steepness $H/L = 0.06$ in cases C1-C3. The wave force on the downstream cylinder 3 in the absence of the upstream cylinder 1 in Fig. (11c) is $0.67F_0$, slightly higher than $0.56F_0$ computed in the presence of the upstream cylinder.

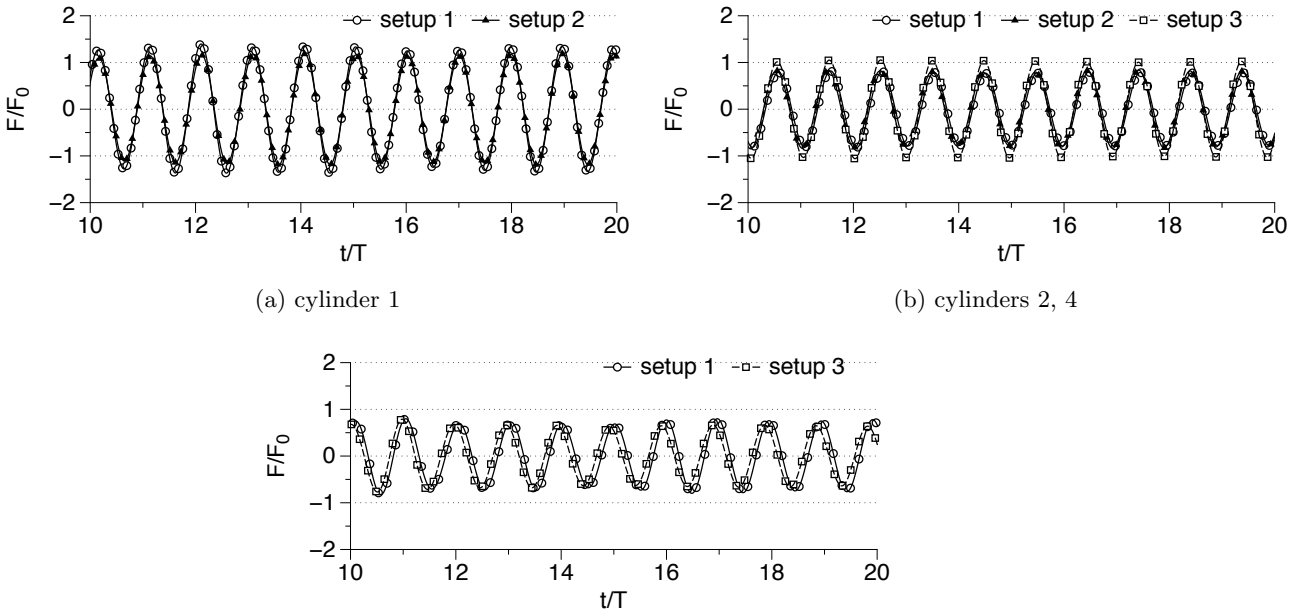

(a) cylinder 1

(b) cylinders 2, 4

(c) cylinder 3

Figure 11: Comparison of wave forces on each of the cylinders in setups E1, E2 and E3 for steepness $H/L = 0.10$ with $H = 0.20$ m and $L = 2.00$ m for $kr = 0.94$

On the increase of the incident wave steepness for an incident wavelength of $L = 2.00$ m,

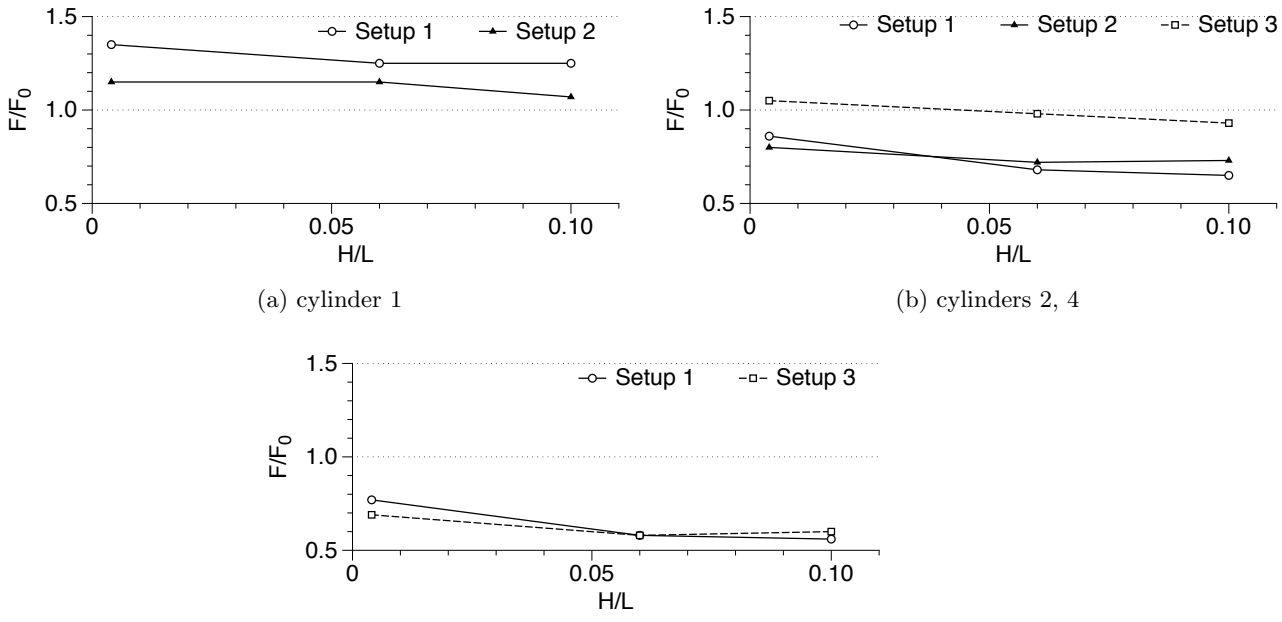

(a) cylinder 1

(b) cylinders 2, 4

(c) cylinder 3

Figure 12: Variation of the wave forces on the cylinders in different setups for different incident wave steepness with $L = 2.00$ m, $kr = 0.94$

the computed wave forces are mostly seen to be lower than the analytical prediction, which match the computed values at the lowest wave steepness of $H/L = 0.004$. This is illustrated in Fig. (12) showing the variation of the wave force with respect to the incident wave steepness, on each cylinder in the different setups presented in this paper. Generally, the ratio F/F_0 reduces as the wave steepness H/L is increased from 0.004 to 0.06. On further increase in the wave steepness to 0.10, the ratio of F/F_0 in each case is either similar to the value at $H/L = 0.06$ or further lowered.

The wave forces computed for cases F1-F3 with an incident wave height of $H = 0.055$ m, wavelength 1.11 m and wave steepness $H/L = 0.1$ are presented in Fig. (13), scaled to the wave force on a single cylinder, $F_0 = 45.5$ N. Figure 13a shows that the force on the upstream cylinder 1 is $1.23F_0$ in the absence of the downstream cylinder in setup 2, while the wave force on cylinder 1 in the presence of the downstream cylinder is lower at $1.02F_0$. In the case of cylinders 2 and 4, the wave forces are $0.90F_0$, $0.82F_0$ and $1.02F_0$ in setups 1, 2 and 3 respectively in Fig. (13b). Cylinders 2 and 4 experience higher forces in the absence of the upstream cylinder in setup 3. The wave force on the downstream cylinder 3 is higher in the absence of the upstream cylinder with forces of $0.67F_0$ and $0.76F_0$ computed in setup 1 and setup 3 respectively, shown in Fig. (13c). The results obtained for this steepness of $H/L = 0.10$ for $L = 1.11$ m are qualitatively similar to the results obtained at $H/L = 0.06$. The variation of the wave forces on each cylinder in the different setups for different incident wave steepness is presented in Fig. (14). A large reduction is seen in the relative wave force on cylinder as the wave steepness is increased from $H/L = 0.004$ to $H/L = 0.06$ due to the breakdown of the wave near-trapping phenomenon in setup 1. Further increase in the wave steepness to 0.10

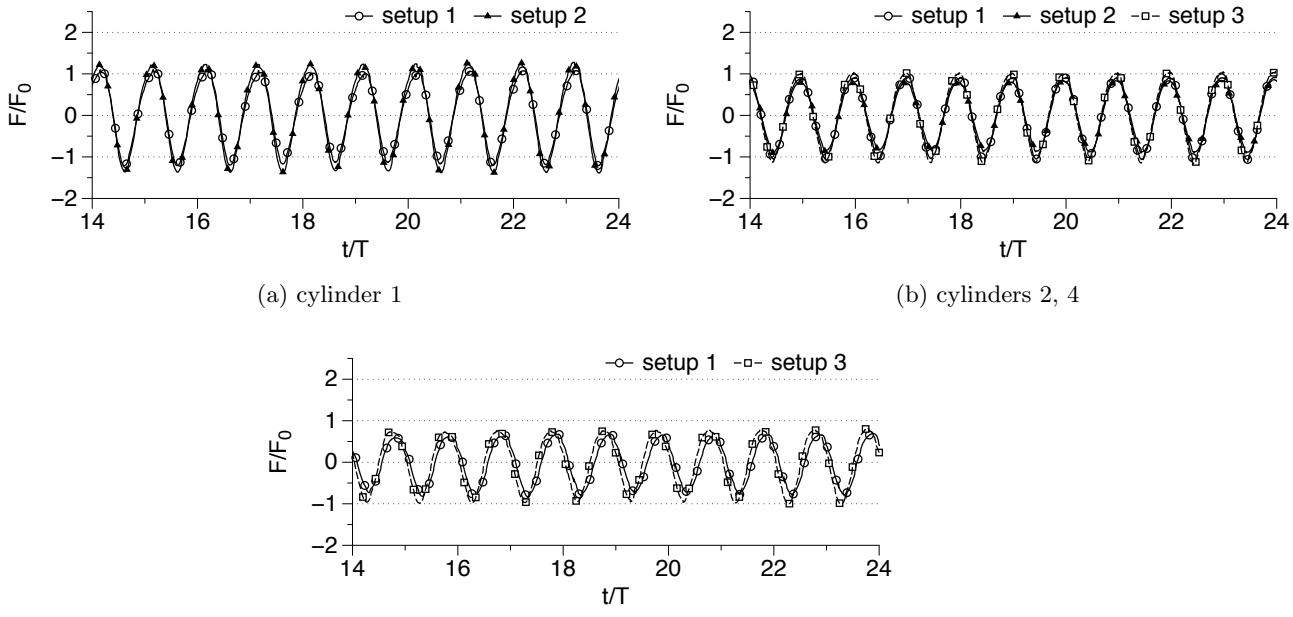

(a) cylinder 1

(b) cylinders 2, 4

(c) cylinder 3

Figure 13: Comparison of wave forces on each of the cylinders in setups F1, F2 and F3 for steepness $H/L = 0.10$ with $H = 0.11$ m and $L = 1.11$ m for $kr = 1.70$

results in some more reduction in the relative wave force on cylinder 1. In setup 2, the change in the relative wave forces on changing the incident wave steepness is not very significant. For cylinders 2 and 4, a slight reduction in the relative wave forces is seen when the wave steepness is increased from $H/L = 0.004$ to 0.06 and on further increase in H/L, the values for F/F_0 do not change significantly. As seen before, the change in the setup have only a minor influence on the wave forces acting on cylinders 2 and 4. The relative wave force on the downstream cylinder 3 is reduced significantly on increasing the incident wave steepness from 0.004 to 0.06 due to the breakdown of the wave near-trapping phenomenon and further increase in H/L leads to a small further reduction. The relative wave forces on cylinder 3 the presence and absence of the upstream cylinder are seen to be similar. This further supports the findings in previous sections that the wave forces on the upstream cylinder are affected due to the presence of the downstream cylinder.

The difference in the wave diffraction regime at low and high incident wave steepnesses is seen from the free surface elevations around the cylinder arrays. This difference results in the different forces seen in the case of high steepness waves than that predicted by analytical formula, that assumes low steepness incident waves. The formation of multiple semi-circular diffracted waves around the cylinders in seen for higher incident wave steepness. On the other hand, in the case of low steepness incident waves, the wave diffraction results in bending of the waveform and for $L = 1.11$ m the phenomenon of near-trapping of waves is observed. The formation of multiple diffracted waves at a higher incident wave steepness results in a break down of the conditions leading to wave near trapping. Since potential theory assumes a low incident wave steepness, formulae based on potential theory cannot account for the diffraction

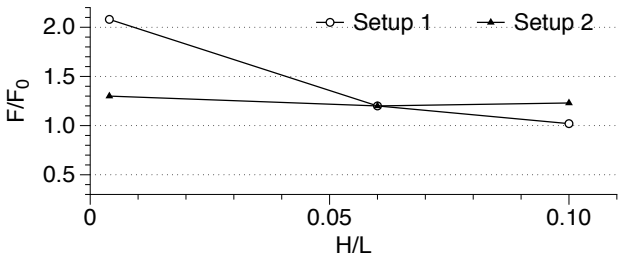

(a) cylinder 1

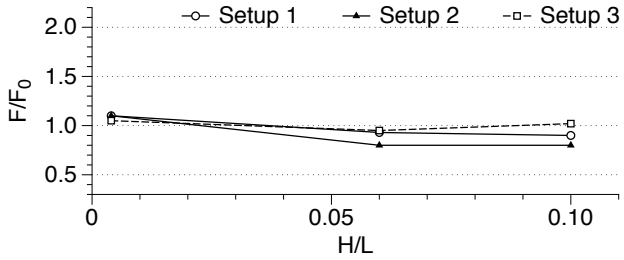

(b) cylinders 2, 4

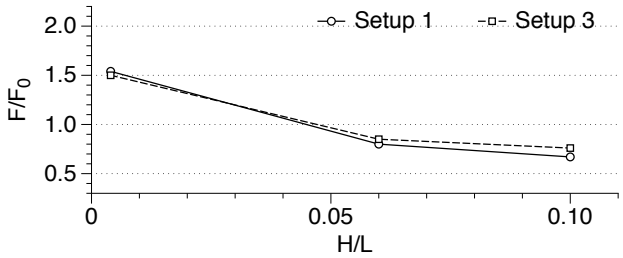

(c) cylinder 3

Figure 14: Variation of the wave forces on the cylinders in different setups for different incident wave steepness with $L = 1.11$ m, $kr = 1.70$

effects at higher wave steepnesses. It is also observed that in the absence of the downstream cylinder 3 in the four cylinder array, the wave forces on the upstream cylinder 1 are reduced.

In the context of an array of oscillating water column wave energy devices, the phenomenon of wave near-trapping could lead to higher free surface oscillations in the vicinity of the devices resulting in higher energy capture. The results presented above, though, show that wave near-trapping breaks down on an increase in the incident wave steepness. Also, the relative wave forces on each of the device is reduced on the increase of incident wave steepness, even at conditions that theoretically lead to wave near-trapping. Thus, for the structural design of the device, wave near-trapping is of concern only at very low incident wave steepness. At higher wave steepnesses, the total force on the device forms the criterion for the structural design of the device. Also, an advantage in terms of potential higher energy capture due to wave near-trapping is only available at a very low incident wave steepness. For further insight into the free surface variations in between the devices and the effect on the energy captured by the devices, further research is needed using a representation of the oscillating water column device in the wave tank.

5 Conclusion

The open source CFD model REEF3D is used to simulate wave interaction with arrays of cylinders to study the change in the hydrodynamics and the wave forces in the presence and absence of cylinders along the the direction of wave propagation. The numerical model was validated using equations based on potential theory for low incident wave steepness for

both a single cylinder and an arrangement of four cylinders. The phenomenon of wave near-trapping resulting in large free surface elevations in the vicinity of the cylinders and large wave forces on the cylinders is observed at low wave steepness in accordance with analytical expectation. The difference in the wave diffraction for different incident wavelengths and wave steepnesses is also studied and found that significant radiating waves are reflected from the cylinders at higher wave steepnesses, which are not observed at lower wave steepnesses. The phenomenon of wave near-trapping is seen to breakdown for higher incident wave steepness due this difference in the diffraction pattern.

The presence of the downstream cylinder generally results in a higher wave force on the upstream cylinder with a 30% increase for low steepness waves and a 60% increase for high steepness waves compared to the force on a single cylinder, at conditions away from theoretical near-wave trapping. Under theoretical conditions for wave near-trapping, the upstream experiences about two times the force on a single cylinder at low steepness and a 20% higher force for high steepness waves. However, at a higher incident wave steepness and break-down of the near-trapping, though the wave forces on the upstream cylinder are the highest in the array, the rest of the cylinders experience lower forces. It can be concluded that the wave interaction with a four cylinder array with a given center-to-center distance depends not only on the incident wavelength but also the incident wave steepness. The effect of higher steepness incident waves cannot be effectively accounted for using formulae based on potential theory. In context of oscillating water column wave energy devices, a potential advantage for higher energy capture due to wave near-trapping is possible only at a very low incident wave steepness. From the structural design point of view of the device, the total force from a higher steepness wave would decide the design requirement and the effect of wave near-trapping can be ignored as it breaks down at a higher incident wave steepness.

6 Acknowledgements

This study has been carried out under the OWCBW project (No. 217622/E20) and the authors are grateful to the grants provided by the Research Council of Norway. This research was supported in part with computational resources at the Norwegian University of Science and Technology (NTNU) provided by NOTUR, http://www.notur.no (NN2620K).

References

Alagan Chella, M., Bihs, H., Myrhaug, D. and Muskulus, M. (2015). Breaking characteristics and geometric properties of spilling breakers over slopes. *Coastal Engineering*, **95**, 4–19.

Barnard, B.J.S., Pritchard, W.G. and Provis, D.G. (1983). Experiments on wave trapping by a submerged cylindrical island. *Geophysical and Astrophysical Fluid Dynamics*, **24**, 23–48.

Berthelsen, P.A. and Faltinsen, O.M. (2008). A local directional ghost cell approach for incompressible viscous flow problems with irregular boundaries. *Journal of Computational Physics*, **227**, 4354–4397.

Chorin, A. (1968). Numerical solution of the Navier-Stokes equations. *Mathematics of Computation*, **22**, 745–762.

Duclos, G. and Clément, A.H. (2004). Wave propagation through arrays of unevenly spaced vertical piles. *Ocean Engineering*, **31**, 1655–1668.

Durbin, P.A. (2009). Limiters and wall treatments in applied turbulence modeling. *Fluid Dynamics Research*, **41**, 1–18.

Evans, D.V. (1978). Oscillating water column wave energy convertors. *IMA Journal of Applied Mathematics*, **22**, 423–433.

Evans, D.V. and Porter, R. (1997). Near-trapping of waves by circular arrays of vertical cylinders. *Applied Ocean Research*, **19**, 83–99.

Hossain, M.S. and Rodi, W. (1980). Mathematical modeling of vertical mixing in stratified channel flow. In: *Proc., 2nd Symposium on Stratified Flows, Trondheim, Norway.*

Huang, J.B. (2004). Nonlinear free surface action with an array of vertical cylinders. *Acta Mechanica Sinica*, **20**(3), 247–262.

Jacobsen, N.G., Fuhrman, D.R. and Fredsøe, J. (2012). A wave generation toolbox for the open-source CFD library: OpenFOAM. *International Journal for Numerical Methods in Fluids*, **70**(9), 1073–1088.

Jiang, G.S. and Peng, D. (2000). Weighted eno schemes for Hamilton-Jacobi equations. *SIAM Journal on Scientific Computing*, **21**, 2126–2143.

Jiang, G.S. and Shu, C.W. (1996). Efficient implementation of weighted ENO schemes. *Journal of Computational Physics*, **126**, 202–228.

Larsen, J. and Dancy, H. (1983). Open boundaries in short wave simulations - a new approach. *Coastal Engineering*, **7**, 285–297.

Linton, C.M. and Evans, D.V. (1990). The interaction of waves with arrays of vertical circular cylinders. *Journal of Fluid Mechanics*, **215**, 549–569.

Linton, C.M. and McIver, P. (2001). *Handbook of mathematical techniques for wave structure interactions.* Chapman and Hall CRC.

MacCamy, R. and Fuchs, R. (1954). *Wave forces on piles: A diffraction theory.* University of California, Dept. of Engineering.

Malenica, S., Taylor, R.E. and Huang, J.B. (1999). Second-order water wave diffraction by an array of vertical cylinders. *Journal of Fluid Mechanics*, **390**, 349–373.

Naot, D. and Rodi, W. (1982). Calculation of secondary currents in channel flow. *Journal of the Hydraulics Division, ASCE*, **108**(8), 948–968.

Ohkusu, M. (1974). Hydrodynamic forces on multiple cylinders in waves. In: *Proc., International Symposium on Dynamics of Marine Vehicles and Structures in Waves, London*, 107–112.

Ohl, C.O.G., Taylor, R.E., Taylor, P.H. and Borthwick, A.G.L. (2001). Water wave diffraction by a cylinder array. Part 1. Regular waves. *Journal of Fluid Mechanics*, **442**, 1–32.

Osher, S. and Sethian, J.A. (1988). Fronts propagating with curvature- dependent speed: algorithms based on Hamilton-Jacobi formulations. *Journal of Computational Physics*, **79**, 12–49.

Peng, D., Merriman, B., Osher, S., Zhao, H. and Kang, M. (1999). A PDE-based fast local level set method. *Journal of Computational Physics*, **155**, 410–438.

Shu, C.W. and Osher, S. (1988). Efficient implementation of essentially non-oscillatory shock capturing schemes. *Journal of Computational Physics*, **77**, 439–471.

Spring, B. and Monkmeyer, P.L. (1974). Interaction of plane waves with vertical cylinders. In: *Proc., International Conference on Coastal Engineering, ASCE, Copenhagen*, 1828–1847.

van der Vorst, H.A. (1992). BiCGStab: A fast and smoothly converging variant of Bi-CG for the solution of nonsymmetric linear systems. *SIAM Journal on Scientific and Statistical Computing*, **13**, 631–644.

Walker, D.A.G. and Taylor, R.E. (2005). Wave diffraction from linear arrays of cylinders. *Ocean Engineering*, **32**, 2053–2078.

Walker, D.A.G., Taylor, R.E., Taylor, P.H. and Zang, J. (2008). Wave diffraction and near-trapping by a multi-column gravity-based structure. *Ocean Engineering*, **35**, 201–209.

Wilcox, D.C. (1994). *Turbulence modeling for CFD.* DCW Industries Inc., La Canada, California.

Zhao, M., Cheng, L. and Teng, B. (2007). Numerical simulation of solitary wave scattering by a circular cylinder array. *Ocean engineering*, **34**(3), 489–499.